Atmospheric Environment 112 (2015) 257–268

Contents lists available at ScienceDirect

Atmospheric Environment

journal homepage: www.elsevier.com/locate/atmosenv

Transport, biomass burning, and in-situ formation contribute to fine particle concentrations at a remote site near Grand Teton National Park

M.I. Schurman [a, *], T. Lee [a, 1], Y. Desyaterik [a], B.A. Schichtel [b], S.M. Kreidenweis [a], J.L. Collett Jr. [a]

[a] Department of Atmospheric Science, Colorado State University, Fort Collins, CO, USA
[b] National Park Service/CIRA, Colorado State University, Fort Collins, CO, USA

HIGHLIGHTS

- Particulate matter at Grand Teton National Park characterized using HR-ToF-AMS.
- In-situ formation of oxygenated OA (61% PM1); transported biomass-burning OA (14%).
- Transport of ammonium (9%) and sulfate (13%) from populated areas to S. and W.
- Daytime organic nitrogen contains nitriles/pyridines, with amine fragments at night.
- Historical data suggest that these characteristics are typical of summer conditions.

ARTICLE INFO

Article history:
Received 25 November 2014
Received in revised form
27 March 2015
Accepted 16 April 2015
Available online 17 April 2015

Keywords:
Organic aerosol
Source apportionment
Secondary organic aerosol
Biomass burning
Background
Organic nitrogen
Aerosol mass spectrometer
Positive matrix factorization

ABSTRACT

Ecosystem health and visibility degradation due to fine-mode atmospheric particles have been documented in remote areas and motivate particle characterization that can inform mitigation strategies. This study explores submicron (PM_1) particle size, composition, and source apportionment at Grand Teton National Park using High-Resolution Time-of-Flight Aerosol Mass Spectrometer data with Positive Matrix Factorization and MODIS fire information. Particulate mass averages 2.08 $\mu g/m^3$ (max = 21.91 $\mu g/m^3$) of which 75.0% is organic; PMF-derived Low-Volatility Oxygenated Organic Aerosol (LV-OOA) averages 61.1% of PM_1 (or 1.05 $\mu g/m^3$), with sporadic but higher-concentration biomass burning (BBOA) events contributing another 13.9%. Sulfate (12.5%), ammonium (8.7%), and nitrate (3.8%) are generally low in mass. Ammonium and sulfate have correlated time-series and association with transport from northern Utah and the Snake River Valley. A regionally disperse and/or *in situ* photochemical LV-OOA source is suggested by 1) afternoon concentration enhancement not correlated with upslope winds, anthropogenic NO_x, or ammonium sulfate, 2) smaller particle size, higher polydispersity, and lower levels of oxidation during the day and in comparison to a biomass burning plume inferred to have traveled ~480 km, and 3) lower degree of oxidation than is usually observed in transported urban plumes and alpine sites with transported anthropogenic OA. CHN fragment spectra suggest organic nitrogen in the form of nitriles and/or pyridines during the day, with the addition of amine fragments at night. Fires near Boise, ID may be the source of a high-concentration biomass-burning event on August 15–16, 2011 associated with SW winds (upslope from the Snake River Valley) and increased sulfate, ammonium, nitrate, and CHN and CHON fragments (nominally, amines and organonitrates). Comparison to limited historical data suggests that the amounts and sources of organics and inorganics presented here typify summer conditions in this area.

1. Introduction

Fine particles are involved in climate and environmental effects including direct and indirect radiative forcing, nutrient deposition,

* Corresponding author. Present address: Division of Environment, Hong Kong University of Science and Technology, Clearwater Bay Rd., Sai Kung, NT, Hong Kong.
E-mail address: mishaschurman.ms@gmail.com (M.I. Schurman).
[1] Now at Department of Environmental Science, Hankuk University of Foreign Studies, Seoul, South Korea.

http://dx.doi.org/10.1016/j.atmosenv.2015.04.043
1352-2310/

visibility degradation, and human health effects, much of which is attributed to anthropogenic emissions (Stocker et al., 2013). As a result, many particle source apportionment studies focus on urban areas. Urban pollution is transported widely into downwind ecosystems (e.g. Van Donkelaar et al., 2008; Zhang et al., 2007), but cities account for only 0.5–2.5% of land surface (Schneider et al., 2010), leaving air quality in many regions uncharacterized. Remote sensing, basic measurement networks such as IMPROVE in the U.S. (Malm and Hand, 2007), and models help to fill in these gaps in terms of particle concentrations, finding that organic aerosol (OA) are a significant fraction of fine particulate mass (Hand et al., 2012; Zhang et al., 2007). However, the sophisticated source apportionment studies need for effective mitigation (and model validation) in remote areas are less common.

Many remote environments are also especially sensitive to nutrient deposition, which can arise from, for example, gaseous or particulate nitrogen species and result in soil nutrient leaching, eutrophication, water-body acidification, and reduced plant hardiness, among other effects (Fenn et al., 2003). Non-nutrient species, such as some organics, can also be involved in chemistry leading to long-range transport and deposition. In Rocky Mountain National Park (RMNP), for instance, deposited nitrogen (mainly in the form of precipitation) is associated with organics transported into the park from neighboring cities (Benedict et al., 2013; Day et al., 2012; Schurman et al., 2015). Fine particles can also contribute to visibility degradation (Levin et al., 2009; Malm and Hand, 2007).

Organic nitrogen (ON) is also of concern, as it comprises roughly one-fifth to one-third of fine particulate mass worldwide and contributes significantly to total nitrogen deposition in RMNP and elsewhere (Cape and Cornell, 2011; Beem et al., 2010). ON compounds found in aerosols include amines and imines, uric, amino, and other organic acids, and organic nitrates (Cape and Cornell, 2011). Like emissions of inorganic nitrogen, which more than doubled since the 1970s, environmental levels of organic nitrogen species have been increasing (Galloway et al., 2008).

At Grand Teton National Park (GTNP), past work indicates large upwind nitrogen emissions (Clarisse et al., 2009) and deposition (Fenn et al., 2003) with clear ecological detriment including lake acidification and diatom species shifts (Saros et al., 2010). The detrimental effects outlined above and lack of prior particle characterization at GTNP motivate the PM_1 source apportionment work presented here.

In general, particle sources in remote areas appear to be complex; biogenic OA is important and often formed from reactions between biogenic volatile organic carbon species (BVOCs) and anthropogenic pollutants (Hoyle et al., 2011); high concentrations of particles and gaseous precursors can also be transported from urban areas. In the RMNP study mentioned above, biomass burning, transport of anthropogenic particles with mountain-valley circulations, and secondary biogenic sources all contributed significantly to fine PM (Schurman et al., 2015); similar patterns have been observed at Whistler Mountain in Canada (Gallagher et al., 2011).

Particle sources can be explored through a combination of composition and meteorological data. For instance, sulfate and nitrate precursors have important anthropogenic sources, and thus if found in an uninhabited area indicate long-range transport. The oxidation level of organic species can also reveal the degree of atmospheric aging. Metrics such as *f*43 (the ratio of mass at *m/z* 43 to total organic mass) and *f*44 (as for *f*43, but for *m/z* 44) are indicative of relative carbonyl/hydrocarbon ($C_2H_3O^+$ and/or $C_3H_7^+$) and carboxylic acid (CO_2^+) content, respectively (Zhang et al., 2011). Ambient aerosols generally progress toward higher *f*44 and lower *f*43 as they are oxidized (Ng et al., 2011). Statistical techniques such as Positive Matrix Factorization are used to explore combinations of aerosol components common at a given site and can be combined with meteorological measurements and/or models to indicate geographical sources of a given particle composition type (Paatero and Tapper, 1994).

However, in order to connect rapid changes in particle composition with meteorological data, the techniques outlined above require higher time resolution than that offered by filter sampling, which can be especially limited (~24 h) in low-mass environments such as GTNP. To this end, an aerosol mass spectrometer with 2–5 min time resolution was deployed as part of the Grand Teton Reactive Nitrogen Deposition Study (GrandTReNDS) with the goal of exploring OA sources, especially as they inform nitrogen deposition. The results are compared to historical particulate matter and fire data to determine whether the particle sources found here represent 'typical' local conditions during summer.

2. Methods

2.1. Instrumentation and analysis

An Aerodyne High-Resolution Time-of-Flight Aerosol Mass Spectrometer (AMS) was used to quantitatively measure the size and non-refractory composition of submicron particles. Briefly, the AMS separates gases and particles by vacuum diffusion differential, separates particle sizes by inertia in a particle flight region, vaporizes the particles at 600 °C, ionizes the fragments under 70 eV electron impact, and detects the ions using time-of-flight mass spectrometry; the AMS has been discussed in depth elsewhere (Decarlo et al., 2006). The aerodynamic lens preceding the interior vacuum transmits particles ~60 nm < D_p < ~700 nm (Liu et al., 2007), encompassing the vast majority of submicron particulate mass measured by a differential mobility particle sizer (DMPS) during this study (Ezra Levin, personal communication, 17 August, 2012; Fig. S1). Co-located instrumentation included a particle sizing rack with an aerodynamic particle sizer (APS, TSI 3021), optical particle counter (OPC, LASAIR 1003), and DMPS (TSI 3085), a gas measurement rack with CO (Teledyne-API Inc., Model 300EU), NO, NO_x, NO_y (Teledyne-API Inc., Models 200EU and Model 201E) and two ammonia (NH_3) measurements (Particle Measuring Systems Air Sentry II Ion Mobility Spectrometer & Picarro G1103 Analyzer), and a Climatronics All-In-One Weather Sensor (Part Number 102780) measuring wind direction and speed, temperature, and relative humidity. 24- and 12-h URG denuder/filter-pack samples were used to characterize gaseous ammonia and nitric acid and $PM_{2.5}$ ion concentrations. Methodological details and results from some of these measurements can be found in Prenni et al. (2014) and Benedict et al. (2013).

The AMS collected 2–5 min average particle mass spectra spanning *m/z* 12- *m/z* 300 for V (high sensitivity), W (high resolution), and PToF (particle sizing) modes (see Decarlo et al., 2006). Ionization efficiency calibrations using 300 nm ammonium nitrate particles were performed once or more per week with verification against an in-line condensation particle counter (CPC, TSI model 3010). Gaseous CO_2 contributions to *m/z* 44 were quantified using an in-line Li-COR CO_2 monitor (LI-820). Data analysis utilized SQUIRREL (v1.51H), PIKA (v1.10H; Sueper, 2013; using the updated fragmentation table from Aiken et al., 2008), and the PMF2 algorithm (Paatero and Tapper, 1994) in PET (v2.03A,Ulbrich et al., 2009) in Igor Pro 6.22A (WaveMetrics Inc., Lake Oswego, OR). High-resolution data are available July 27 19:00 through the end of the study.

Quantifying organic nitrogen via AMS is complicated by the ionization-induced fragmentation of nominally 'nitrate' (NO_n^+) and 'ammonium' (NH_n^+) ions from organic parent compounds (broadly, organonitrates and amines, respectively) under ionization (Farmer

et al., 2010; Rollins et al., 2010). Fortunately, some nominally organic-nitrogen fragments in the CHN (~amine) and CHON (~organonitrate) families are often preserved; from these it is sometimes possible to identify classes of compounds present from fragmentation patterns. The total mass of the CHN and CHON fragments also provides a lower bound on the ON concentration (ON_{min}).

Positive Matrix Factorization (PMF) is a positivity-constrained, receptor-only, least-squares regression algorithm used to deconvolve the time series of organic mass spectra into a user-selected number of spectrally-static organic 'factors' whose contributions to total organic mass vary over time (Paatero and Tapper, 1994; Paatero, 1997). Data preparation followed Ulbrich et al. (2009) and Zhang et al. (2011) and included fragments $\leq m/z$ 110. Due to low mass, the signal-to-noise threshold under which fragments are considered 'weak' and are down-weighted, normally equal to 2, was reduced to 1.2 to achieve Q/Qexp = 1.06 (S:N < 1.2: down-weight factor = 2; S:N < 0.2: fragment excluded; Paatero and Hopke, 2003). One-to four-factor solutions were explored while varying FPEAK from −1 to 1. A two-factor solution was selected based on criteria outlined in the literature, including spectral dissimilarities, timeline dissimilarities and correlations with other stracers, comparison to 'established' factor types (Ulbrich et al., 2009), and lack of improvement in statistics such as residuals with greater factor number (Figs. S2 and S3); FPEAK = 0.4 best resolves the BBOA factor, which should increase only when biomass burning marker *f*60 (*m/z* 60/total organic mass) exceeds the background level of 0.003 and contain all *m/z* 60 mass above background levels (Cubison et al., 2011).

Associations between particle constituent concentrations and meteorology are explored using simple wind-rose plots with raw concentrations and averages over each of 16 cardinal bins. The Conditional Probability Function (CPF) identifies wind directions contributing high constituent concentrations by dividing the number of concentrations points greater than a threshold measured in a given wind sector by the number of data points in that sector (Kim and Hopke, 2004); here, thresholds are the species average plus one standard deviation. Back-trajectory information using the Hybrid Single Particle Lagrangian Integrated Trajectory (HYSPLIT) model from an associated paper is used to support conclusions drawn from basic meteorological analysis above (Benedict et al., 2013).

2.2. Sampling site

The Grand Teton sampling site was located at 2722 m (8930 ft) near the summit of Peaked Mountain, just outside the western boundary of Grand Teton National Park on a west-facing slope looking over the Snake River Valley (lat.: 43.7928° N, lon.: 110.9592° W, Fig. 1). The closest sizeable population is Driggs, ID (population = 1660 in 2011), approximately 16 km (10 mi) away at the foot of the mountain; Idaho Falls (metropolitan population = 136,108 in 2011) is ~93 km (58 mi) distant. Instruments were housed in a mobile laboratory parked at the top of the Sacajawea Ski Lift of the Grand Targhee Ski Resort. This site was one of eleven in the wider Grand Teton Reactive Nitrogen Deposition Study (GrandTReNDS) aimed at quantifying regional air pollution and reactive nitrogen sources and deposition in Grand Teton National Park; measurements were conducted 25 July − 31 August, 2011.

Meteorological and gas-phase data illustrate prevalent conditions and transport at the site (Fig. 2, Prenni et al., 2014). Diurnal hourly averages of wind direction reveal steady SSE winds (~175°) overnight (22:00–09:00 LST) that shift abruptly to the WSW (~250°) direction in the morning and afternoon (10:00–21:00 LST); this is characteristic of the thermally driven mountain-valley circulations common in such terrain (Bossert et al., 1989). NO_x is produced primarily by human activities; NO_x enhancement at the onset of the daytime upslope wind suggests the import of anthropogenically-influenced air masses (through thermal upslope flow and/or boundary layer expansion) and is mirrored in gaseous ammonia, which features noon-time enhancement in both Picarro and Air Sentry instrument measurements, though the ammonia maximum may be enhanced by thermally-driven partitioning to the gas phase during the heat of the day. These patterns suggest boundary layer influence during the day, while nighttime concentration decreases ensue from cleaner downslope transport, as explored later.

Maximum particle number concentration occurs at ~17:00 LST, lagging well behind the beginning of the upslope winds (Prenni et al., 2014). This particle number increase could arise from import of aerosols formed or emitted in the valley during the day or from in-situ formation, as may be indicated in the AMS size and composition data discussed later. Lastly, HYSPLIT back-trajectories during the study period reveal dominant transport routes through the Snake River Valley (SW) and from the northern Utah/southern Wyoming area (SE; Benedict et al., 2013, Fig. 1 in Prenni et al., 2014).

3. Results

3.1. General particle composition and concentration

Atmospheric submicron particles at the sampling site are generally low in mass concentration and consist primarily of organics, with two periods of enhanced (>[avg. + std. dev.]) concentration coinciding with regional wildfires (total organics: 5-min max. = 17.98 μg/m^3; avg. = 1.56 ± 1.19 μg/m^3 or 75.0% of average AMS mass). Inorganic species are lower in concentration; sulfate (max. = 1.00 μg/m^3; avg. = 0.26 ± 0.12 μg/m^3) and ammonium (max. = 0.78 μg/m^3; avg. = 0.18 ± 0.06 μg/m^3) are more abundant in general than nitrate (max. = 2.14 μg/m^3, avg. = 0.078 ± 0.12 μg/m^3; the nitrate V-mode detection limit ≈0.003 μg/m^3; Decarlo et al., 2006; Drewnick and Hings, 2009). Increased nitrate concentrations are accompanied by increased organic mass (Fig. 3). These values compare well to co-located 24-h URG measurements (Fig. S6). The closest site with which to compare these data is the Yellowstone National Park IMPROVE station, ~65 km (~40 miles) and across the Teton range from the site presented here, at which filter samples are collected every third day. July–August average concentrations over 1996–2012 are: organic mass = 3.90 ± 6.11 μg/m^3, calculated via 1.8*organic carbon (Malm and Hand, 2007); nitrate = 0.10 ± 0.10 μg/m^3; sulfate = 0.46 ± 0.21 μg/m^3; ammonium = 0.07 ± 0.05 μg/m^3 (not measured, but calculated as that needed to neutralize sulfate and nitrate); and $PM_{2.5}$ = 5.04 ± 3.78 μg/m^3, statistically like those observed here using a Wilcoxon Rank test. Yellowstone organics generally feature ~1 high-concentration event (>10 μg/m^3) each summer (July–August).

Internal aerosol mixtures may be indicated by correlated time-series; in the AMS data, nitrate and total organics are correlated (r^2 = 0.86), as are ammonium and sulfate (r^2 = 0.70), for which the mass ratio of NH_4 to SO_4 = 0.41. The stoichiometric slope for pure ammonium sulfate by mass is 0.38, suggesting that ammonium sulfate, which is formed preferentially compared to ammonium nitrate, may be an important form of both ammonium and sulfate. However, there are also periods in which the concentration of ammonium equals or exceeds that needed to neutralize sulfate; during these episodes, ammonium fragments may arise from ammonium nitrate, amines, carboxylate-ammonium salts such as

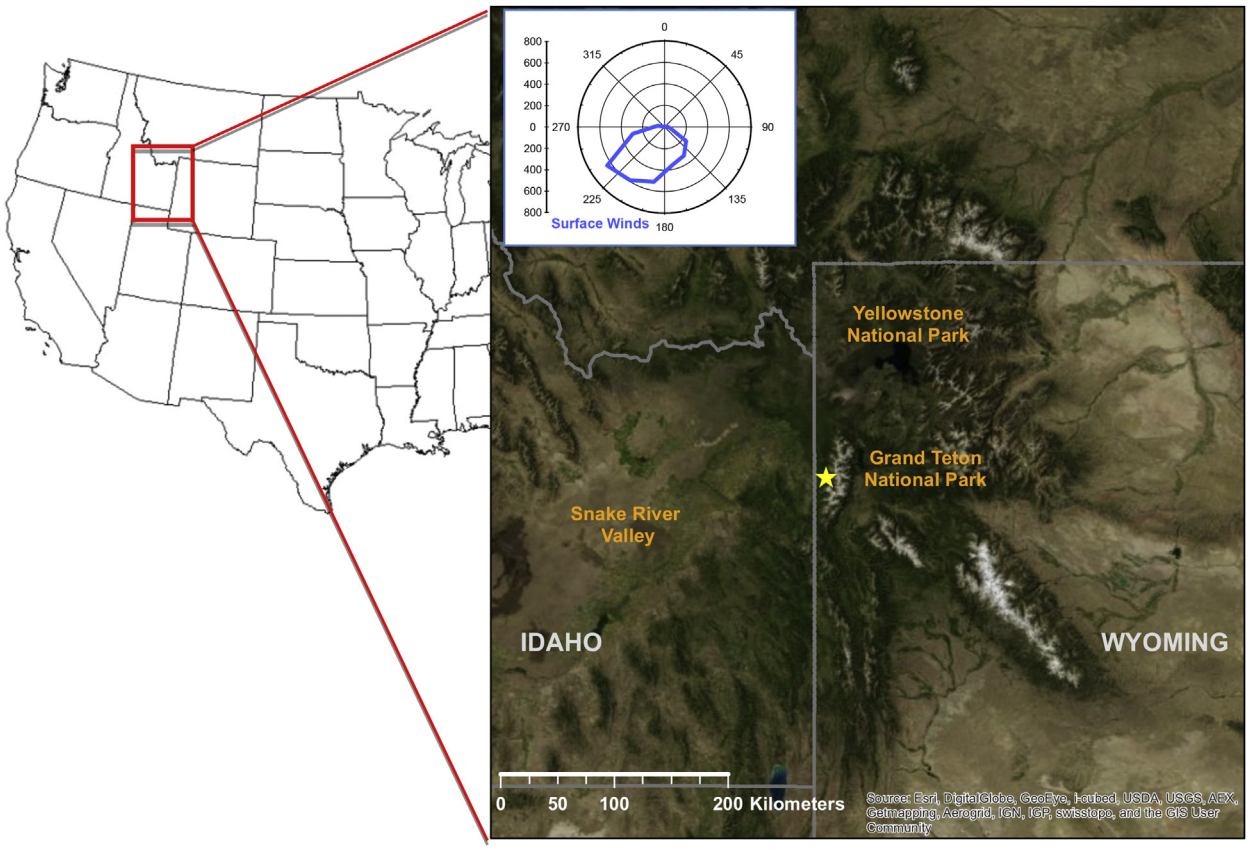

Fig. 1. Map showing GrandTReNDS study site (yellow star) and a histogram of surface wind direction counts during the study (ARCgis map generation: Zitely Tzompa, 15 March 2014). (For interpretation of the references to colour in this figure legend, the reader is referred to the web version of this article.)

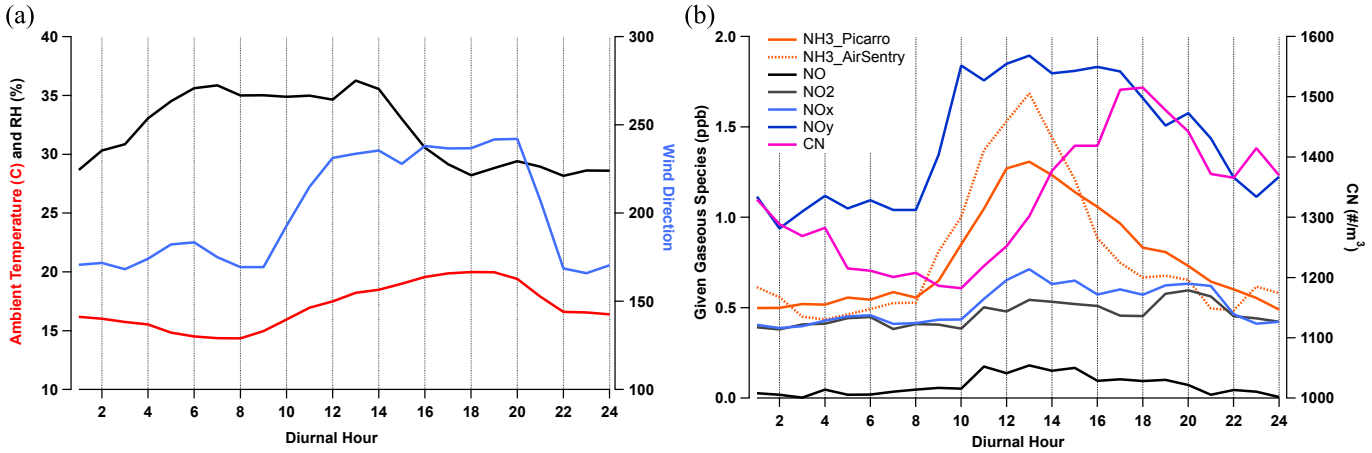

Fig. 2. Diurnal averages of a) meteorological values ambient temperature (°C), relative humidity (%), and wind direction (degrees), and b) gaseous NH_3, NO, NO_x, and NO_y concentrations (ppb) and particle number concentration (CN; #/m^3; distribution from combined DMPS, OPC, and APS data). These observations are discussed in detail in Prenni et al. (2014).

ammonium oxalate, etc. as discussed in Section 3.4 (Malm et al., 2005). 'Excess' ammonium (NH_4^*) is calculated as the mass of ammonium exceeding that in stoichiometric balance with sulfate.

NH_4^* is weakly correlated with nitrate and often has a similar time series (Table 1); at other times, NH_4^* may exceed stoichiometric balance with nitrate, indicating possible amine and/or organic ammonium salt contributions, or vice versa, suggesting enhanced organonitrates or soil-influenced species such as calcium nitrate (though the effect of refractory calcium on AMS vaporization of calcium nitrate has not been discussed in the literature; Lee et al., 2004). Fig. 4 shows the relationship between NH_4^* and NO_3 colored by concentration of organics. Most data points lie above the line of ammonium-nitrate stoichiometry, indicating excess ammonium fragments and possible amine content. Data below the line are indicative of excess nitrate fragments (and possible organonitrate content) and occur only when [Org] > ~8 μg/m^3, during an August 15 biomass burning event identified by PMF; this pattern is also observed in URG filter data

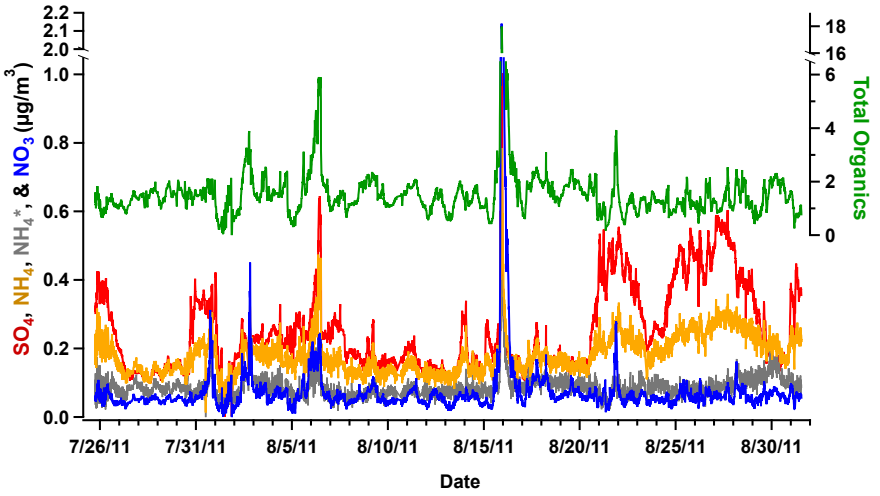

Fig. 3. Timeline of total organics (green, right axis), sulfate (red), ammonium (yellow), nitrate (dark blue), and 'excess' ammonium (NH_4^*, grey) from the HR-ToF-AMS during the GrandTReNDS study. Concentrations (μg/m^3) are 2–5 min averages. (For interpretation of the references to colour in this figure legend, the reader is referred to the web version of this article.)

Table 1
Coefficients of determination (r^2) between temporal concentration variations of given particle constituent pairs; NH_4^* refers to mass of ammonium exceeding that in stoichiometric balance with sulfate. ON_{min} is defined in Section 2.1.

	LV-OOA	BBOA	SO_4	NO_3	Total organics
SO_4	0.00	0.04			0.02
NO_3	0.46	0.90	0.04		0.86
NH_4	0.12	0.27	0.70	0.27	0.23
NH_4^*	0.31	0.45	0.02	0.46	0.50
ON_{min}	0.01	0.25			

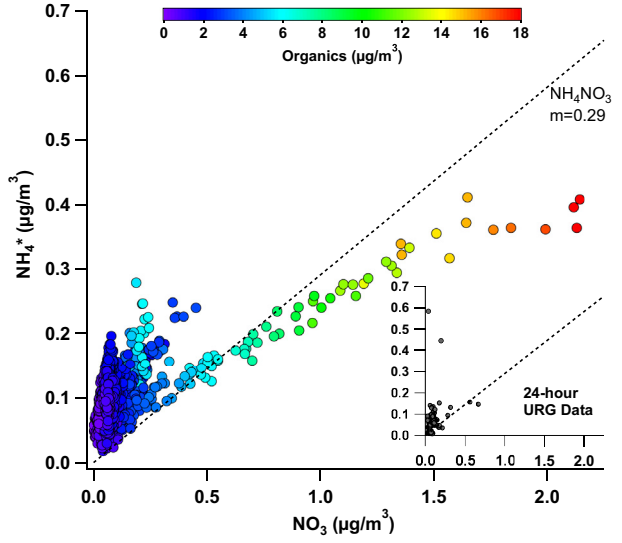

Fig. 4. Ammonium in excess of charge balance with sulfate (NH_4^*) versus nitrate. The dashed line indicates the stoichiometric mass ratio of pure ammonium nitrate. The inset shows the same components, with the same axes, from co-located 24-h URG filter (with a backup denuder for volatilized ammonium) samples. URG data courtesy Katie Benedict; see Benedict et al. (2013) for methodological details.

(Fig. 4, inset). Lastly, the lack of correlation between other species combinations may indicate external mixture between ammonium-sulfate and organic/ammonium*-nitrate particle types (or, at least, unrelated sources and transport; Table 1).

Both ammonium and sulfate have a weak average diurnal maximum in the afternoon, when winds are from the SW, with another slightly higher maximum overnight when winds are from the SE (Fig. 5); the 75th percentile concentrations follow similar patterns for both species, indicating that higher concentrations occur consistently and are not strongly influenced by outliers. The mean nitrate concentration has a maximum at 23:00 LST without commensurate 25th and 75th percentile increases, indicating that the mean is driven by low-frequency, high-concentration events (in this case, the August 15 biomass burning episode). Total organics increase consistently and significantly in the afternoon (mode at 15:00 LST), with another event-driven mean maximum at ~23:00 LST; these patterns are examined in depth below.

3.2. PMF-derived organic aerosol factors

A two-factor PMF solution was indicated by good reconstruction of mass (within ±5% of total organics) and the failure of additional factors to produce meaningful differences in mass spectra (Fig. 6), time series (Fig. 7), or diurnal profiles (Fig. 5); see supplement.

A Low-Volatility Oxidized Organic Aerosol (LV-OOA) factor is identified by the predominance of mass at *m/z* 44 (CO_2^+, some $C_2H_4O^+$) over that at *m/z* 43 ($C_2H_3O^+$ and $C_3H_7^+$, Zhang et al., 2011), while a Biomass-Burning OA (BBOA) factor features prominent fragments of anhydrosugars from cellulose combustion, such as levoglucosan, at *m/z* 60 ($C_2H_4O_2^+$) and *m/z* 73 ($C_3H_5O_2^+$) (Alfarra et al., 2007). *f*60 (*m/z* 60/total organic mass) allows convenient comparison to other BBOA factors in the literature; herein, $f60_{BB\ factor}$ = 0.008, well beyond the "background" value (0.003) + 3σ ≈ 0.005, lower than fresh emissions (~0.01–0.04; Grieshop et al., 2009), and consistent with plumes aged 3–24 h from 245 BB plumes sampled during the ARCTAS campaign ($f60_{median}$ ≈ 0.008) and other aged biomass burning plumes in the literature (Cubison et al., 2011 and references therein).

LV-OOA dominates submicron particulate organic mass (max. = 5.32 μg/m^3; avg. = 1.05 ± 0.48 μg/m^3, Fig. 7), contributing 61% of average particle mass and 81% of average organic mass, with a consistent, significant diurnal maximum in the midafternoon (~15:00 LST, Fig. 5) but few other episodic features. This afternoon increase could be driven: a) by photochemistry, which can produce condensable SVOCs from gaseous precursors (e.g., biogenic VOCs from nearby forests); b) by transport from the nearby Snake River

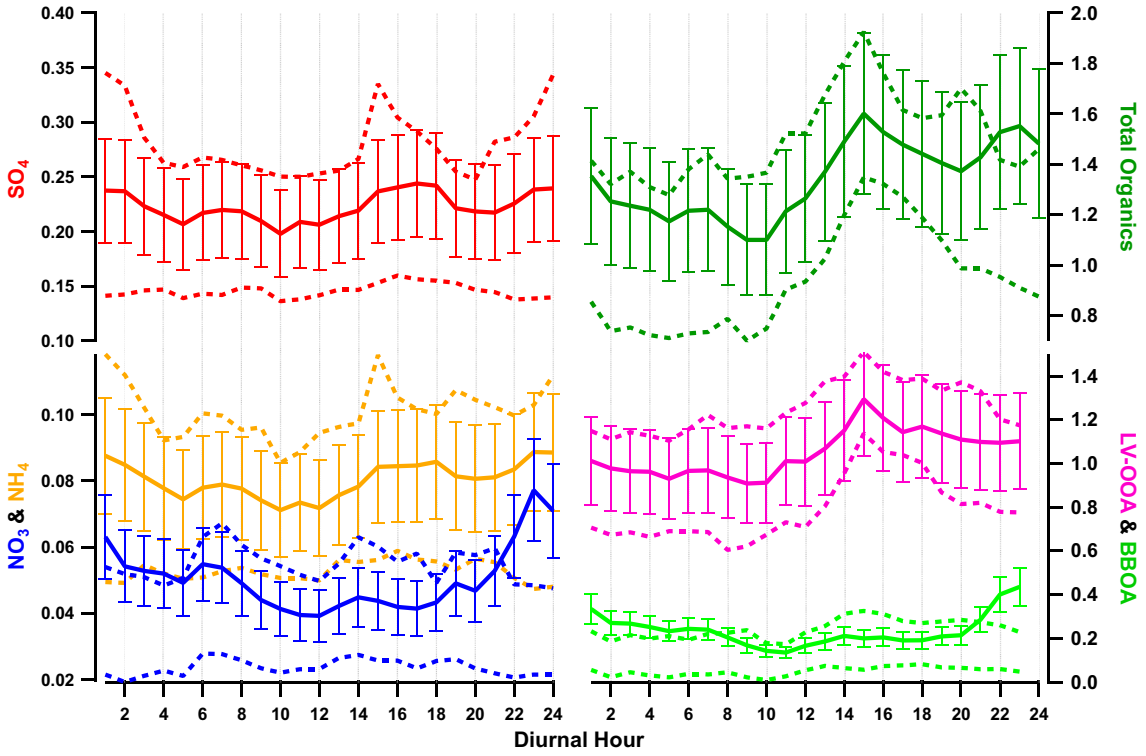

Fig. 5. Study-average diurnal concentrations (μg/m^3) of inorganic species, total organics, and organic PMF factors (introduced below), where the solid line is the concentration mean and the dashed lines are 25th and 75th percentiles. Error bars represent ~20% mass quantification error in the AMS.

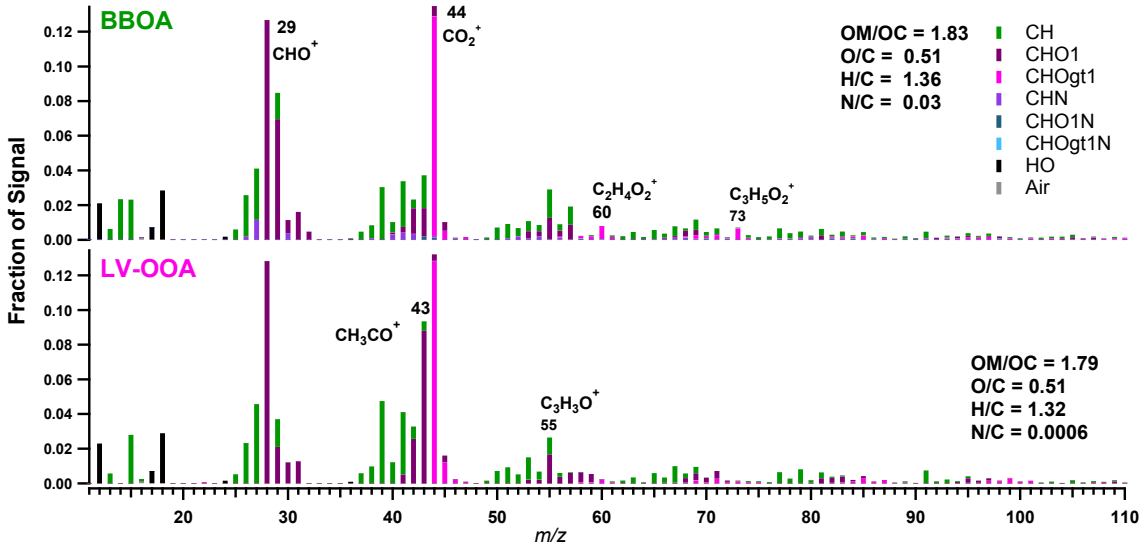

Fig. 6. Mass spectra of LV-OOA and BBOA factors derived from application of PMF to high-resolution Grand Teton National Park AMS data; colored bars show the signal contributed by the indicated fragment family at a given *m/z*. (For interpretation of the references to colour in this figure legend, the reader is referred to the web version of this article.)

Valley by the consistent upslope flow beginning at ~9:00 LST; and/or c) by boundary layer fluctuations, in which the BL expands to encompass the sampling site, bringing with it generally higher particle concentrations (Gallagher et al., 2011). The diurnal pattern of LV-OOA begins to increase at a similar time as does NO_x (10:00 LST), which might suggest anthropogenic air-mass impact, but LV-OOA is not like NO_x in diurnal profile, nor is it correlated to NO_x ($r^2 = 0.001$); LV-OOA has a weak correlation with nitrate, another semivolatile species (Table 1). Organic composition measured at the site is fairly static, with little variation in the organic mass spectrum as represented by fragment ratios *f*43 and *f*44 apart from the biomass burning events described later.

Biomass burning OA is dominant during wildfire events on August 15 and 21 and comprises 14% of average particle mass and 19% of total organic mass on average (max. = 9.03 μg/m^3; avg. = 0.24 ± 0.62 μg/m^3); historically, 2011 was a relatively low fire year in Idaho, with ~20 Gg carbonaceous aerosol emitted ($PM_{2.5}$) against the 2002–2012 average of 30 ± 40 Gg (Val Martin et al.,

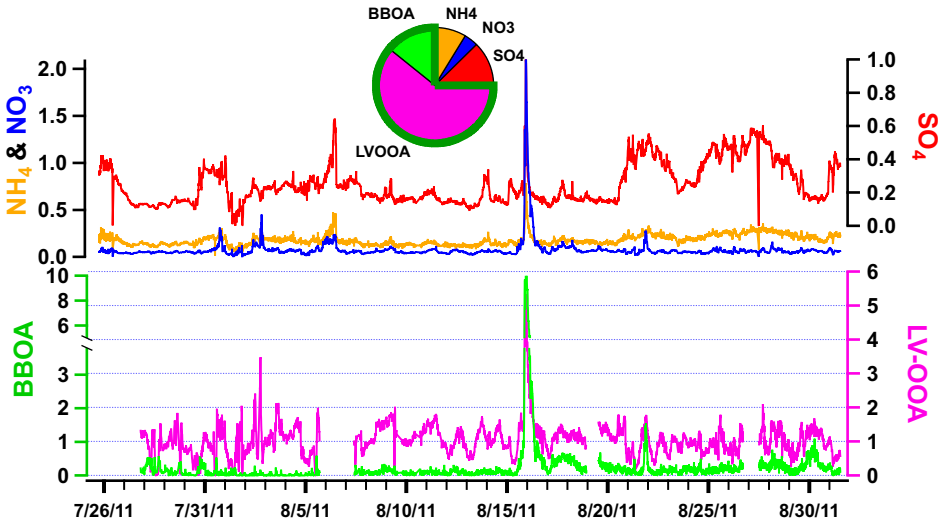

Fig. 7. Timelines of LV-OOA (pink) and BBOA (green) PMF organic factors and inorganics at the Grand Teton site, in μg/m^3. The pie chart depicts study average mass contributions from each component, with total organics outlined in green. (For interpretation of the references to colour in this figure legend, the reader is referred to the web version of this article.)

2013). From MODIS data, the only fire activity around August 15 and within the HYSPLIT back-trajectory source regions (Benedict et al., 2013) was a cluster of large fires SE of Boise, including the South Pen, Union, Squaw, Blair, Big Hill, and Morrow fires spanning August 14–16 with 77,000 burnt acres combined (Forest Service Remote Sensing Application Center database, USFS (2013), Fig. S6); these were approximately 480 km (~300 mi) from the site at the other end of the Snake River Valley, which may conduct surface flow toward the site.

The August 15 episode drives a BBOA diurnal mean maximum at ~23:00 LST that is not reflected in the 25th or 75th percentiles, indicating that BBOA follows no consistent diurnal pattern; BBOA at this site is episodic, consistent with sporadic regional fires and generally low BBOA background concentrations (Fig. 7). An internal mixture of BBOA and (nominally inorganic) nitrate fragments is indicated by correlated time-series ($r^2 = 0.90$ with NO_3), diurnal patterns, particle size (Section 3.5), and wind association (Section 3.6), but BBOA is not correlated with ammonium or sulfate.

In the *f*43-*f*44 triangle diagram (Fig. 8; Ng et al., 2011), the majority of the data fall in the SV-OOA (grey ellipse)/LV-OOA (pink ellipse) overlap region, indicating a somewhat static level of oxidation over the study period. The August 15 biomass-burning event, which spanned ~19:15 LST August 15 (with sunset at 20:49 LST) and ending at ~09:40 August 16 (with sunrise at 06:50 LST), is shown colored by time. Oxidation decreases as the event progresses, which may have a variety of causes including decreased transport times toward the event end (though wind speed did not change significantly), reduction in photochemical oxidation after the sun set, condensation of less-oxidized SVOCs onto the new particle surface area in the plume, or a change in aggregate fire phase and/or combustion efficiency (Weimer et al., 2008).

Finally, throughout this paper, in order to explore continuous OA variability despite the static nature of PMF factors, periods dominated by a given factor will be identified and subject to various analyses; "BBOA-dominated" episodes when [BB] $\geq$ 0.40 μg/m^3), which neatly encompasses the two biomass burning events mentioned in the text, and "LV-dominated" episodes include all other periods (noting that the BBOA factor was near zero for all time periods except the few events outlined in the text).

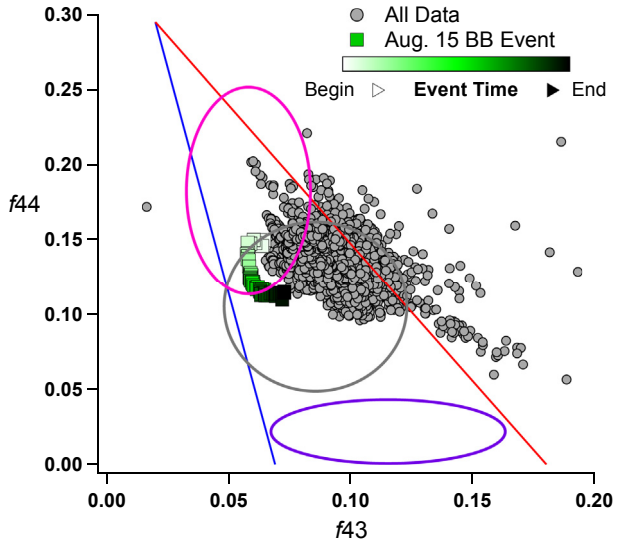

Fig. 8. *f*43 versus *f*44 diagram featuring the August 15, 2011 biomass burning event. Ellipses indicate the typical ranges of HOA (purple), SV-OOA (grey), and LV-OOA (pink) data in the literature (Ng et al., 2011). (For interpretation of the references to colour in this figure legend, the reader is referred to the web version of this article.)

3.3. Elemental analysis of the carbonaceous fraction

The ratio of organic matter to organic carbon (OM:OC) may be used as a metric of aerosol oxidation and averages 1.78 ± 0.10 in total and 1.79 for the LV-OOA PMF factor. Aiken et al. (2008) found a similar value (~1.8) for their PMF-derived Semi Volatile-OOA factor from a site near Mexico City, but higher values (~1.9–2.1) as the plume traveled to more remote regions; OM:OC for urban aerosols typically measure ~1.3–1.6, while values of 2–2.5 have been observed at rural sites with anthropogenic influence (Aiken et al., 2008; Turpin and Lim, 2001). Likewise, the LV-OOA mass spectrum at Grand Teton has greater relative signal at *m/z* 43 (indicating relatively less oxidized organic components) in comparison to LV-OOA at many remote sites, including Rocky Mountain National

Park, where organics were partly transported from nearby urban areas (Schurman et al., 2015). Given the distance from major population centers, this OM:OC value implies that Tetons OOA may not arise solely from transported anthropogenic particles, which we might expect to be more aged, but may be influenced by, for example, condensation of SVOCs from local forests onto particles; it is also possible that oxidation per unit time during transport is reduced in comparison to those studies, due to lower oxidant concentrations.

The August 15 biomass burning event has an average OM:OC of 1.78 ± 0.07; OM:OC = 1.83 for the BBOA PMF factor. These values are slightly higher than (indicating relative oxidation) or consistent with those observed during biomass burning events in the literature, many of which were urban and/or in closer proximity to the burn and measured OM:OC = 1.6–1.7 (Aiken et al., 2008; Chen et al., 2009; Turpin and Lim, 2001); for instance, BBOA in Rocky Mountain National Park emitted ~200 m–0.5 km from the measurement site measured OM:OC = 1.76 ± 0.12 (Schurman et al., 2015).

The elemental ratio of oxygen to carbon (O:C) averages 0.49 ± 0.08 (PMF LV-OOA: 0.51; PMF BBOA: 0.51) and is, again, more consistent with published SV-OOA factors than LV-OOA (Aiken et al., 2008; Ng et al., 2010; Huang et al., 2011). In contrast, at Whistler Mountain in British Colombia, organic aerosol transported ~100 km from the Vancouver urban area had an O:C of 1.08, while OA from mixtures of transport and local biogenic sources measured O:C = 0.65–0.69 (Sun et al., 2009). O:C averaged during the biomass burning events is not significantly different than the total average (avg_{BB} = 0.49 ± 0.05), but both this value and that of the PMF BBOA factor are higher than other published BBOA events (~0.26–0.4, which usually spent less time in transport than in this case), reflecting greater oxidation during transport and/or the ubiquity of OOA at this site (Aiken et al., 2008; Huang et al., 2011).

H:C averages 1.36 ± 0.10, between SV-OOA and LV-OOA values (Aiken et al., 2008; Ng et al., 2010) and lower than that measured in urban primary OA (Aiken et al., 2008; Huang et al., 2011). For the PMF factors, LV-OOA has an H:C = 1.32 while BBOA H:C = 1.36. Organic aerosol N:C averages 0.017 ± 0.020 (max = 0.30 during the Aug. 15 biomass burning event, avg_{BB} = 0.012 ± 0.004) and is higher in the BBOA factor than the LVOOA factor, indicating nominally organic nitrogen content (CHON and CHN fragments) in the biomass burning events; these average values are on the higher end of the range found in the literature, which contains no value over N:C = 0.09 for a field campaign to our knowledge (Aiken et al., 2008; Huang et al., 2011). Elemental ratios do not vary between day and night (not shown). This static OA composition is more consistent with a ubiquitous ('regional background') *in situ* source than it would be with transported plumes, and may also indicate that the site does not regularly enter the free troposphere.

3.4. Organic nitrogen

There is evidence of organonitrate and amine species in Grand Teton aerosol. Nominally organonitrate fragments ($C_xH_yO_zN^+$ family, 'CHON' hereafter) form clear 'wave'-like mass spectral patterns, which arise from successive fragmentation of methylene bridges (–CH_2–). However, the signal intensity of these fragments is about 100 times lower than that for other organics ($C_xH_y^+$ and $C_xH_yO_z^+$ families). The sum of CHON fragment mass yields an average $ON_{min,\ CHON}$ of 0.01 ± 0.01 μg/m^3 (maximum = 0.12 μg/m^3 or 0.7% of total OM during BBOA periods), which is at the detection limit for the W mode. Though fragment signal is enhanced during the Aug. 15 BBOA event, there is little variation in CHON mass spectral patterns throughout the study. However, the association between nominally inorganic nitrate in excess of that stoichiometrically balanced with NH_4^* and biomass burning events (which are often associated with nitrophenols, etc., Desyaterik et al., 2013) suggests that some of the nitrate may arise from organonitrates.

CHN ions are more abundant (Fig. 9), with about two times the signal intensity of the CHON family. Unlike CHON, CHN fragments vary over time in both signal intensity and mass spectral patterns. CHN fragments are more abundant during the daytime, and the average daytime spectrum contains a $C_XH_5N^+$ series at *m/z*s 55, 67, 79, and 91 indicative of nitrile and/or pyridine-type fragments (which have the same empirical formula) in 70 eV reference spectra, which are generally comparable to fragmentation in the AMS (NIST Webbook; Alfarra, 2004); unfortunately, the possibility of several parent compounds contributing to a given fragment preclude compound identification. Pyridine compounds are abundant in tropospheric particles and emitted from combustion and soil, with an atmospheric lifetime of ~5–59 days allowing wide dispersion (Atkinson et al., 1987); while pyridine is fairly volatile, absorption may occur in the presence of sufficient organic substrate (Schulte and Arnold, 1990). A number of nitriles are used as herbicides; regional agriculture could be a source of both compound types.

The daytime CHN spectrum ("pyridines/nitriles") differs from published spectra of, for example, common ambient component trimethylamine (*m/z*s 30, 58, 72, and 86, etc.; Silva et al., 2008) and chamber amine SOA experiments (*m/z*s 30, 31, 58, 88, and 118 for various amine precursors; Murphy et al., 2007). However, some of these amine fragments are enhanced in the nighttime average spectrum; of particular note is CH_4N^+ at *m/z* 30, which is a common amine fragment (McLafferty and Turecek, 1993). During the August 15 biomass burning event, total CHN signal is 2.25 times larger than for the average of the remainder of the study period, whereas as total organic signal is enhanced by a factor of 4.87 (on average). Following the CHON analysis, average $ON_{min,CHN}$ = 0.03 ± 0.03 μg/m^3 (max = 0.34 μg/m^3); giving a total average $ON_{min} = ON_{min,CHN} + ON_{min,\ CHON}$ = 0.04 μg/m^3 (max = 0.43 μg/m^3).

3.5. Particle size

Due to low particle mass concentrations, average size distributions were calculated for the study entire, daytime, nighttime, and periods dominated by a given PMF factor as defined earlier. IGOR lognormal fits of these average size distributions allow better statistical comparison between given conditions and allow size estimation for low-signal species such as nitrate (Fig. 10). Ammonium is omitted due to high noise in the size distributions causing difficulty in lognormal fitting.

Particles were notably larger (geometric mean diameter ≈ 250 nm) and more monodisperse (as indicated by the geometric standard deviation) during BBOA events, suggesting an aged aerosol, as particles undergoing atmospheric processing generally become larger and more monodisperse via condensation and coagulation (Reid et al., 2005). The size distribution of organics during the BBOA event was bimodal, as shown in Supplemental Fig. S6, with a minor mode comprising 22.1% of total organic mass with a mode at 613 nm; average mass spectra of both modes contained biomass burning markers *m/z* 60 and *m/z* 73 (Fig. S7). In contrast, the smaller size (mode ≈ 200–210 nm) and relative polydispersity of background aerosol ('day' and 'night' in Fig. 10; 'all' includes BBOA events), suggests fresher particles; this is consistent with the hypothesis presented earlier that local formation may be more important than transport for LV-OOA. The daytime aerosol is slightly smaller and more polydisperse than during the night, which could arise from photochemical formation. Sulfate, which is thought to be transported from anthropogenic sources, is

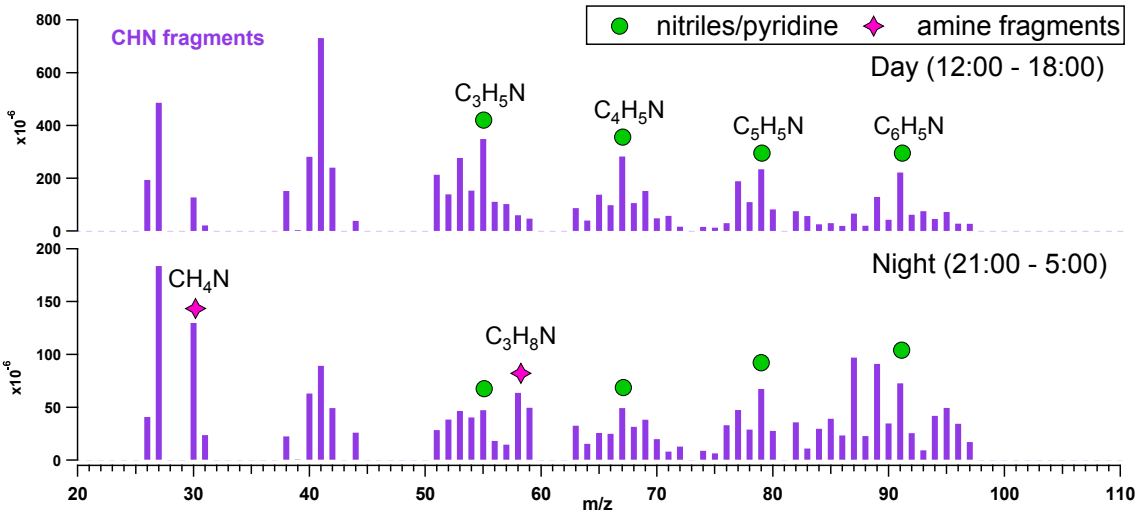

Fig. 9. Mass spectra of $C_xH_yN^+$ fragments averaged over all runs for the indicated time period during the Grand Tetons campaign.

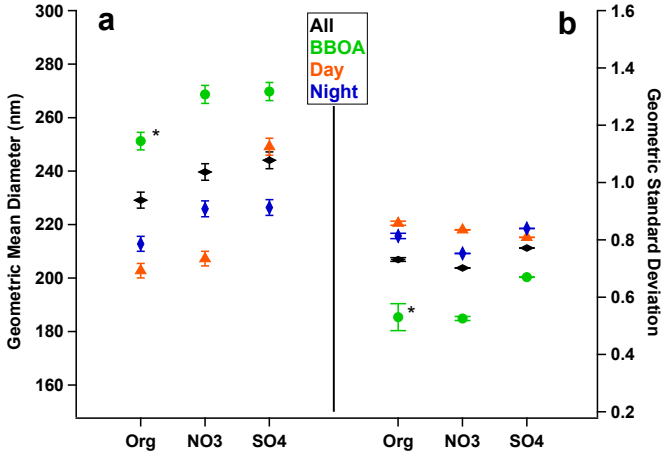

Fig. 10. For the lognormal fit of the average mass size distribution for the given component (text marker) and time period (color): a) the geometric mean diameter (with error bars equaling estimated size-dependent PToF error, compounding chopper broadening and calibration-particle size standard deviation, in nm; see supplement) and b) the geometric standard deviation (σ_g, with error bars equaling the reduced chi-squared value, representing goodness of lognormal fit). 'BBOA' data averaged over the biomass burning event spanning ~19:15 LST August 15 to ~09:40 August 16; 'Day' data averaged over 12:00–18:00 LST; 'Night' data averaged over 21:00–5:00 LST. *The geometric mean diameter and standard deviation shown here are for the major mode (77.9% of total mass) of the two modes found in the size distribution of organics during the BBOA event and the reduced chi-squared is for the entire lognormal fitting using the IGOR multipeak fitting package V2.16; see supplement. (For interpretation of the references to colour in this figure legend, the reader is referred to the web version of this article.)

larger during the day than organics and nitrate, indicating an external mixture during that time, on average.

3.6. Meteorological analysis

The evidence shown so far for transported BBOA and locally-formed and/or 'regional background' LV-OOA can be supported by relating component concentrations to wind direction and HYSPLIT back-trajectories. Wind roses with raw data, average concentrations over 16 wind bins, and conditional probability functions (CPF) are shown in Fig. 11. LV-OOA concentrations are constant with respect to wind direction at ~1.5 μg/m^3, aside from a few higher values from the SSW during the biomass burning event; this consistency is reflected in the average concentration trace and the CPF, which suggests no directionality apart from high values to the NNE and NNW, which are a function of the low wind counts in those bins (a caveat to using CPF). Lastly, the episodic, transported nature of BBOA is reflected in a few scattered high-concentration events in the raw data (including the Aug. 15 biomass burning plume to the SSW) with CPFs near zero (Fig. 11).

In contrast, both ammonium and sulfate show enhanced raw, average, and CPF traces with S–SE wind, which is approximately parallel to the plane of the mountain's slope (Fig. 11); in concomitant measurements presented in Benedict (2012; Appendix G), HYSPLIT back-trajectories during periods of increased ammonia and nitric acid gas concentrations show both a) transport from the Snake River Valley, consistent with upslope wind patterns and weak afternoon increases in inorganics herein, and b) origins in northern Utah (Salt Lake City)/southern Wyoming with subsequent transport across the Tetons from the S/SE, consistent with the sulfate and ammonium CPF patterns above; both sources are indicated for sulfate and ammonium herein, though the Utah/Wyoming source contributes higher concentrations. For all inorganic species, high CPF values from the NE (and NW for nitrate) may come from low wind bin counts and/or sporadic complex transport sourced in the Snake River Valley or Utah and traveling to Yellowstone before turning south, as indicated in Benedict (2012). Lastly, daytime boundary layer influence is clear in this and concomitant datasets; for nighttime, while increases in ammonium and sulfate could come from free tropospheric influence (as well as the HYSPLIT-indicated transport from Utah/Wyoming), the fact that OA elemental analysis does not vary diurnally whatsoever suggests a constant boundary layer influence.

3.7. Summary and conclusions

Summer non-refractory submicron particulate mass at GTNP averages 2.08 μg/m^3 of which 75.0% is organic; sulfate contributes 12.5% of total mass on average, with lower ammonium (8.7%) and nitrate (3.8%). Ammonium and sulfate are correlated, with conditional probability functions indicating predominant transport from northern Utah/southern Wyoming; weak afternoon concentration maxima associated with upslope winds also suggest some ammonium and sulfate transport from the Snake River valley. HYSPLIT

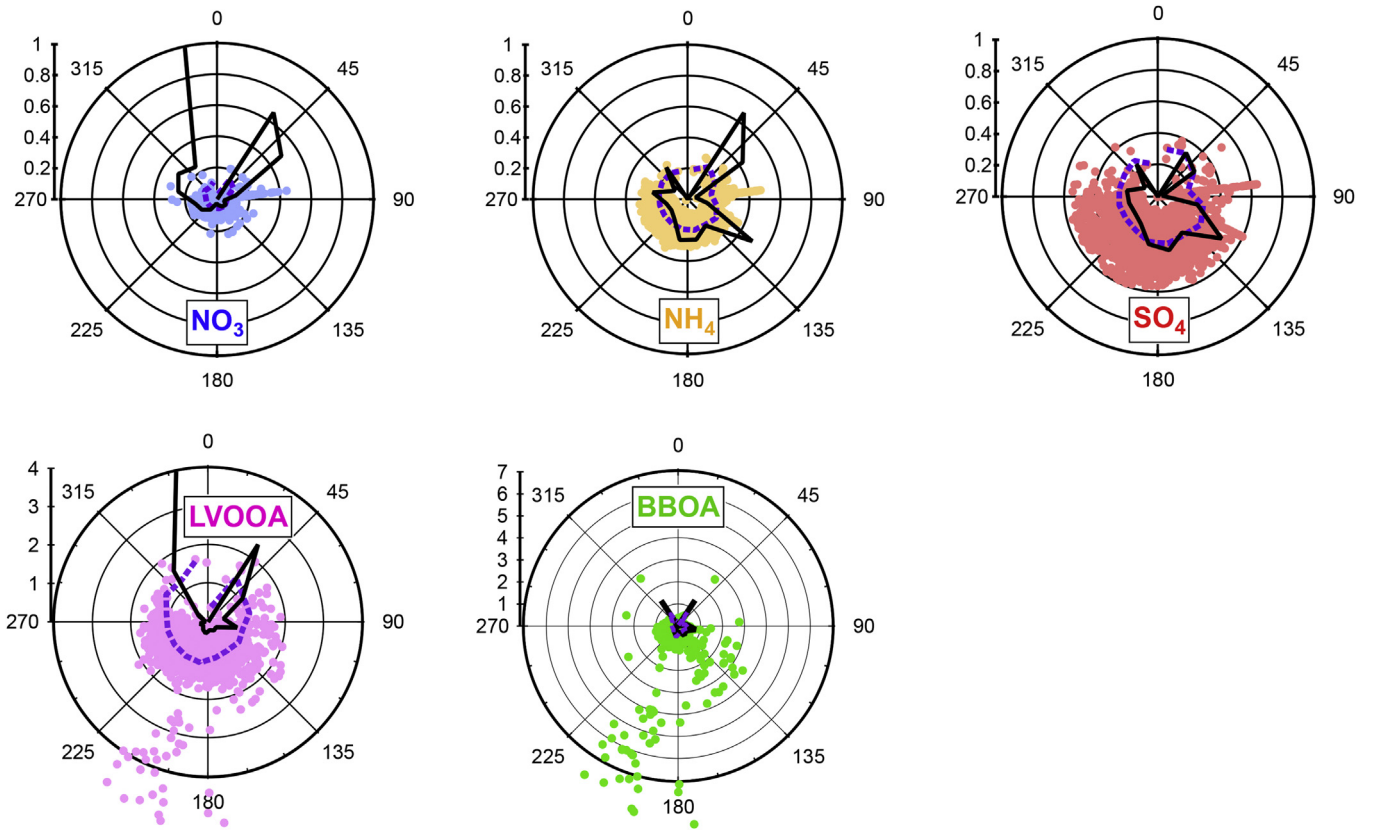

Fig. 11. Wind roses showing raw component concentration (colored by given component, in μg/m^3), concentration average within each of 16 wind bins (dashed purple line, in μg/m^3), and conditional probability function in each bin (solid black line); PMF-factor CPFs have been scaled for direct comparability with inorganic CPFs via multiplication by the given radial axis maximum. (For interpretation of the references to colour in this figure legend, the reader is referred to the web version of this article.)

back-trajectories support both source regions.

PMF analysis of the organic mass spectra indicates two organic aerosol types: 'background' low-volatility oxidized organic aerosol (LV-OOA) and episodic biomass burning aerosol (BBOA). LV-OOA contributes ~61.1% of total mass on average, with fairly static mass spectral composition and concentrations (usually ~0.5–1.5 μg/m^3). Though mass at *m/z* 44 is greater than that at *m/z* 43 (which is the definition of 'LV-OOA'), OM:OC, O:C, and data placement in *f*43 vs. *f*44-space indicate that the data overlap typical SV-OOA and LV-OOA ranges, a relatively lower degree of oxidation than is often observed in highly aged urban plumes and alpine sites with transported anthropogenic OA. LV-OOA is enhanced in the afternoon along with particle number concentration, but not correlated with upslope winds, anthropogenic NO_x, or ammonium sulfate; LV-OOA at the site is also smaller and more polydisperse a) during the day, and b) in comparison to a biomass burning plume inferred to have traveled ~480 km. These patterns suggest the importance of *in situ* photochemical OA formation and/or growth (perhaps from local biogenic VOCs), though transported anthropogenic OA and/or gaseous precursors cannot be excluded if they are regionally disperse.

A high-concentration biomass-burning OA episode on August 15–16, 2011 is thought to be transported from fires near Boise, ID. This event is associated with SW winds (upslope from the Snake River Valley) and increased sulfate; enhanced ammonium*, nitrate, and CHN and CHON fragment abundance (nominally, amine and organonitrate compounds), suggest enhanced organic nitrogen content. Particles were larger and more monodisperse during this time period, consistent with extended transport and oxidation time.

CHN-fragment spectra indicated nitrile and/or pyridine content during the day with the addition of amine fragments at night. The constant presence of CHON fragments suggests that organonitrates (or other compounds fragmenting to CHON) are part of the regional LV-OOA background. Agriculture abounds locally and may contribute both amines (though natural sources are also possible) and pyridines/nitriles; photochemical oxidation reactions (in particular of biogenic SVOCs) may result in organonitrates. Based on limited historical data, the amounts and sources of organics and inorganics appear to represent 'typical' summer conditions in this area.

Acknowledgments

This study was supported by National Park Service grant H2370094000/P11AT70958. We would like to thank Amy Sullivan, Katherine Benedict, Derek Day, Yi Li, and Ezra Levin for their extensive support in the field.

Appendix A. Supplementary data

Supplementary data related to this article can be found at http://dx.doi.org/10.1016/j.atmosenv.2015.04.043.

References

Aiken, A.C., Decarlo, P.F., Kroll, J.H., Worsnop, D.R., Huffman, J.A., Docherty, K.S., , et al.Jimenez, J.L., 2008. O/C and OM/OC ratios of primary, secondary, and ambient organic aerosols with high-resolution time-of-flight aerosol mass spectrometry. Environ. Sci. Technol. 42 (12), 4478–4485.

Alfarra, M.R., 2004. Insights into Atmospheric Organic Aerosols Using an Aerosol

Mass Spectrometer. University of Manchester Institute of Science and Technology.
Alfarra, M.R., Prevot, A.S.H., Szidat, S., Sandradewi, J., Weimer, S., Lanz, V.A., , et al.Baltensperger, U., 2007. Identification of the mass spectral signature of organic aerosols from wood burning emissions. Environ. Sci. Technol. 41 (16), 5770–5777.
Atkinson, R., Tuazon, E.C., Wallington, T.J., Aschmann, S.M., Arey, J., Winer, A.M., Pitts, J.N., 1987. Atmospheric chemistry of aniline, N,N-dimethylaniline, pyridine, 1,3,5-triazine, and nitrobenzene. Environ. Sci. Technol. 21 (1), 64–72. http://dx.doi.org/10.1021/es00155a007.
Beem, K.B., Raja, S., Schwandner, F.M., Taylor, C., Lee, T., Sullivan, A.P., , et al.Collett, J.L., 2010. Deposition of reactive nitrogen during the rocky mountain airborne nitrogen and sulfur (RoMANS) study. Environ. Pollut. 158 (3), 862–872. http://dx.doi.org/10.1016/j.envpol.2009.09.023.
Benedict, K.B., 2012. Observations of Atmospheric Reactive Nitrogen Species and Nitrogen Deposition in the Rocky Mountains. Colorado State University, Fort Collins, CO.
Benedict, K.B., Chen, X., Sullivan, A.P., Li, Y., Day, D., Levin, E., Prenni, A., Kreidenweis, S.M., Schichtel, B., Collett Jr., J.L., 2013. The spatial distribution of reactive nitrogen species and nitrogen deposition in Grand Teton National Park. J. Geophys. Res. 118 (11), 875–887.
Bossert, J.E., Sheaffer, J.D., Reiter, E.R., 1989. Aspects of regional-scale flows in mountainous terrain. J. Appl. Meteorol. (United States) 28, 7.
Cape, J.N., Cornell, S., Jickells, T., Nemitz, E., October 2011. Organic nitrogen in the atmosphere—Where does it come from? A review of sources and methods. Atmos. Res. 102 (1–2), 30–48.
Chen, Q., Farmer, D.K., Schneider, J., Zorn, S.R., Heald, C.L., Karl, T.G., , et al.Martin, S.T., 2009. Mass spectral characterization of submicron biogenic organic particles in the Amazon Basin. Geophys. Res. Lett. 36 (20), L20806. http://dx.doi.org/10.1029/2009GL039880.
Clarisse, L., Clerbaux, C., Dentener, F., Hurtmans, D., Coheur, P.-F., 2009. Global ammonia distribution derived from infrared satellite observations. Nat. Geosci. 2 (7), 479–483. http://dx.doi.org/10.1038/ngeo551.
Cubison, M.J., Ortega, A.M., Hayes, P.L., Farmer, D.K., Day, D., Lechner, M.J., , et al.Jimenez, J.L., 2011. Effects of aging on organic aerosol from open biomass burning smoke in aircraft and lab studies. Atmos. Chem. Phys. Discuss. 11 (4), 12103–12140. http://dx.doi.org/10.5194/acpd-11-12103-2011.
Day, D.E., Chen, X., Gebhart, K.A., Carrico, C.M., Schwandner, F.M., Benedict, K.B., , et al.Collett, J.L., 2012. Spatial and temporal variability of ammonia and other inorganic aerosol species. Atmos. Environ. 61 (null), 490–498. http://dx.doi.org/10.1016/j.atmosenv.2012.06.045.
Decarlo, P.F., Kimmel, J.R., Trimborn, A., Northway, M.J., Jayne, J.T., Aiken, A.C., , et al.Jimenez, J.L., 2006. Field-deployable, high-resolution, time-of-flight aerosol mass spectrometer. Anal. Chem. 78 (24), 8281–8289. http://dx.doi.org/10.1021/ac061249n.
Desyaterik, Y., Sun, Y., Shen, X., Lee, T., Wang, X., Wang, T., Collett, J.L., 2013. Speciation of "brown" carbon in cloud water impacted by agricultural biomass burning in eastern China. J. Geophys. Res. Atmos. 118 (13), 7389–7399. http://dx.doi.org/10.1002/jgrd.50561.
Drewnick, F., Hings, S., 2009. Aerosol quantification with the aerodyne aerosol mass spectrometer: detection limits and ionizer background effects. Atmospheric 2006, 33–46.
Farmer, D.K., Matsunaga, A., Docherty, K.S., Surratt, J.D., Seinfeld, J.H., Ziemann, P.J., Jimenez, J.L., 2010. Response of an aerosol mass spectrometer to organonitrates and organosulfates and implications for atmospheric chemistry. Proc. Natl. Acad. Sci. 107, 6670–6675.
Fenn, M.E., Baron, J.S., Allen, E.B., Rueth, H.M., Nydick, K.R., Geiser, L., , et al.Neitlich, P., 2003. Ecological effects of nitrogen deposition in the western United States. BioScience 53 (4), 404.
Gallagher, J.P., McKendry, I.G., Macdonald, A.M., Leaitch, W.R., 2011. Seasonal and diurnal variations in aerosol concentration on Whistler Mountain: boundary layer influence and synoptic-scale controls. J. Appl. Meteorol. Climatol. 50 (11), 2210–2222. http://dx.doi.org/10.1175/JAMC-D-11-028.1.
Galloway, J.N., Townsend, A.R., Erisman, J.W., Bekunda, M., Cai, Z., Freney, J.R., Martinelli, L.A., Seitzinger, S.P., Sutton, M.A., 2008. Transformation of the nitrogen cycle: recent trends, questions, and potential solutions. Science 320 (5878), 889–892. http://dx.doi.org/10.1126/science.1136674.
Grieshop, A.P., Donahue, N.M., Robinson, A.L., 2009. Laboratory investigation of photochemical oxidation of organic aerosol from wood fires 2: analysis of aerosol mass spectrometer data. Atmos. Chem. Phys. 9 (6), 2227–2240. http://dx.doi.org/10.5194/acp-9-2227-2009.
Hand, J.L., Schichtel, B.A., Pitchford, M., Malm, W.C., Frank, N.H., 2012. Seasonal composition of remote and urban fine particulate matter in the United States. J. Geophys. Res. 117 (D5), D05209. http://dx.doi.org/10.1029/2011JD017122.
Hoyle, C.R., Boy, M., Donahue, N.M., Fry, J.L., Glasius, M., Guenther, A., , et al.Sullivan, A.P., 2011. A review of the anthropogenic influence on biogenic secondary organic aerosol. Atmos. Chem. Phys. 11 (1), 321–343. http://dx.doi.org/10.5194/acp-11-321-2011.
Huang, X.-F., He, L.-Y., Hu, M., Canagaratna, M.R., Kroll, J.H., Ng, N.L., , et al.Worsnop, D.R., 2011. Characterization of submicron aerosols at a rural site in Pearl River Delta of China using an aerodyne high-resolution aerosol mass spectrometer. Atmos. Chem. Phys. 11 (5), 1865–1877. http://dx.doi.org/10.5194/acp-11-1865-2011.
Kim, E., Hopke, P.K., 2004. Comparison between conditional probability function and nonparametric regression for Fine particle source directions. Atmos. Environ. 38 (28), 4667–4673. http://dx.doi.org/10.1016/j.atmosenv.2004.05.035.
Lee, T., Kreidenweis, S.M., Collett, J.L., 2004. Aerosol ion characteristics during the Big Bend regional aerosol and visibility observational study. J. Air Waste Manag. Assoc. (1995) 54 (5), 585–592.
Levin, E.J.T., Kreidenweis, S.M., McMeeking, G.R., Carrico, C.M., Collett Jr., J.L., Malm, W.C., 2009. Aerosol physical, chemical and optical properties during the rocky mountain airborne nitrogen and sulfur study. Atmos. Environ. 43 (11), 1932–1939. http://dx.doi.org/10.1016/j.atmosenv.2008.12.042.
Liu, P.S.K., Deng, R., Smith, K.A., Williams, L.R., Jayne, J.T., Canagaratna, M.R., , et al.Deshler, T., 2007. Transmission efficiency of an aerodynamic focusing lens system: comparison of model calculations and laboratory measurements for the aerodyne aerosol mass spectrometer. Aerosol Sci. Technol. 41 (8), 721–733. http://dx.doi.org/10.1080/02786820701422278.
Malm, W.C., Day, D.E., Carrico, C.M., Kreidenweis, S.M., Collett, J.L., McMeeking, G.R., , et al.Schichtel, B.A., 2005. Intercomparison and closure calculations using measurements of aerosol species and optical properties during the Yosemite Aerosol characterization study. J. Geophys. Res. 110 (D14), D14302. http://dx.doi.org/10.1029/2004JD005494.
Malm, W.C., Hand, J.L., 2007. An examination of the physical and optical properties of aerosols collected in the IMPROVE program. Atmos. Environ. 41 (16), 3407–3427.
McLafferty, F.W., Turecek, F., 1993. Interpretation of Mass Spectra, fouth ed. University Science Books, Herndon, VA.
Murphy, S.M., Sorooshian, A., Kroll, J.H., Ng, N.L., Chhabra, P., Tong, C., , et al.Seinfeld, J.H., 2007. Secondary aerosol formation from atmospheric reactions of aliphatic amines. Atmos. Chem. Phys. Discuss. 7 (1), 289–349. http://dx.doi.org/10.5194/acpd-7-289-2007.
Ng, N.L., Canagaratna, M.R., Jimenez, J.L., Chhabra, P.S., Seinfeld, J.H., Worsnop, D.R., 2011. Changes in organic aerosol composition with aging inferred from aerosol mass spectra. Atmos. Chem. Phys. 11 (13), 6465–6474. http://dx.doi.org/10.5194/acp-11-6465-2011.
Ng, N.L., Canagaratna, M.R., Zhang, Q., Jimenez, J.L., Tian, J., Ulbrich, I.M., , et al.Worsnop, D.R., 2010. Organic aerosol components observed in northern hemispheric datasets from aerosol mass Spectrometry. Atmos. Chem. Phys. 10 (10), 4625–4641. http://dx.doi.org/10.5194/acp-10-4625-2010.
Paatero, P., 1997. Least squares formulation of robust non-negative factor analysis. Chemom. Intell. Lab. Syst. 37 (1), 23–35.
Paatero, P., Hopke, P.K., 2003. Discarding or downweighting high-noise variables in factor analytic models. Anal. Chim. Acta 490 (1–2), 277–289. http://dx.doi.org/10.1016/S0003-2670(02)01643-4.
Paatero, P., Tapper, U., 1994. Positive matrix factorization: a non-negative factor model with optimal utilization of error estimates of data values. Environmetrics 5 (2), 111–126.
Prenni, A.J., Levin, E.J.T., Benedict, K.B., Sullivan, A.P., Schurman, M.I., Gebhart, K.A., , et al.Kreidenweis, S.M., 2014. Gas-phase reactive nitrogen near Grand Teton National Park: impacts of transport, anthropogenic emissions, and biomass burning. Atmos. Environ. 89, 749–756. http://dx.doi.org/10.1016/j.atmosenv.2014.03.017.
Reid, J.S., Koppmann, R., Eck, T.F., Eleuterio, D.P., 2005. A review of biomass burning emissions part II: intensive physical properties of biomass burning particles. Atmos. Chem. Phys. 5 (3), 799–825. http://dx.doi.org/10.5194/acp-5-799-2005.
Rollins, A.W., Fry, J.L., Hunter, J.F., Kroll, J.H., Worsnop, D.R., Singaram, S.W., Cohen, R.C., 2010. Elemental analysis of aerosol organic nitrates with electron ionization high-resolution mass spectrometry. Atmos. Meas. Tech. 3 (1), 301–310. http://dx.doi.org/10.5194/amt-3-301-2010.
Saros, J.E., Clow, D.W., Blett, T., Wolfe, A.P., 2010. Critical nitrogen deposition loads in high-elevation lakes of the western US inferred from paleolimnological records. Water Air Soil Pollut. 216 (1–4), 193–202. http://dx.doi.org/10.1007/s11270-010-0526-6.
Schneider, A., Friedl, M.A., Potere, D., 2010. Mapping global urban areas using MODIS 500-m data: new methods and datasets based on "urban ecoregions. Remote Sens. Environ. 114 (8), 1733–1746. http://dx.doi.org/10.1016/j.rse.2010.03.003.
Schulte, P., Arnold, F., 1990. Pyridinium ions and pyridine in the free troposphere. Geophys. Res. Lett. 17 (8), 1077–1080. http://dx.doi.org/10.1029/GL017i008p01077.
Schurman, M.I., Lee, T., Sun, Y., Schichtel, B.A., Kreidenweis, S.M., Collett Jr., J.L., 2015. Investigating types and sources of organic aerosol in rocky mountain National Park using aerosol mass spectrometry. Atmos. Chem. Phys. 15, 737–752. http://dx.doi.org/10.5194/acp-15-737-2015.
Silva, P.J., Erupe, M.E., Price, D., Elias, J., Malloy, Q.G.J., Li, Q., , et al.Cocker, D.R., 2008. Trimethylamine as precursor to secondary organic aerosol formation via nitrate radical reaction in the atmosphere. Environ. Sci. Technol. 42 (13), 4689–4696.
Stocker, T.F., Qin, D., Plattner, G.-K., Tignor, M., Allen, S.K., Boschung, J., , et al.Midgley, P.M., 2013. Climate Change 2013: the Physical Science Basis (Contribution of Working Group I to the Fifth Assessment Report of the Intergovernmental Panel on Climate Change. Cambridge, United Kingdom and New York, NY, USA).
(accessed 2013) Sueper, D., 2013. ToF-AMS Analysis Software Web Page. http://cires.colorado.edu/jimenez-group/ToFAMSResources/ToFSoftware/SquirrelInfo/.
Sun, Y., Zhang, Q., Macdonald, A.M., Hayden, K., Li, S.M., Liggio, J., , et al.Martin, R.V., 2009. Size-resolved aerosol chemistry on Whistler Mountain, Canada with a high-resolution aerosol mass spectrometer during INTEX-B. Atmos. Chem. Phys. 9 (9), 3095–3111. http://dx.doi.org/10.5194/acp-9-3095-2009.
Turpin, B.J., Lim, H.-J., 2001. Species contributions to $PM_{2.5}$ mass concentrations:

revisiting common assumptions for estimating organic mass. Aerosol Sci. Technol. 35 (1), 602–610. http://dx.doi.org/10.1080/02786820119445.

Ulbrich, I.M., Canagaratna, M.R., Zhang, Q., Worsnop, D.R., Jimenez, J.L., 2009. Interpretation of organic components from positive matrix factorization of aerosol mass spectrometric data. Atmos. Chem. Phys. 9 (9), 2891–2918. http://dx.doi.org/10.5194/acp-9-2891-2009.

USFS, 2013. USFS Remote Sensing Applications Center MODIS Fire Mapping Database. Retrieved May 23, 2013, from. http://activefiremaps.fs.fed.us/activefiremaps.php.

Val Martin, M., Heald, C.L., Ford, B., Prenni, A.J., Wiedinmyer, C., 2013. A decadal satellite analysis of the origins and impacts of smoke in Colorado. Atmos. Chem. Phys. 13 (15), 7429–7439. http://dx.doi.org/10.5194/acp-13-7429-2013.

Van Donkelaar, A., Martin, R.V., Leaitch, W.R., Macdonald, A.M., Walker, T.W., Streets, D.G., , et al.Andreae, M.O., 2008. Analysis of aircraft and satellite measurements from the Intercontinental Chemical Transport Experiment (INTEX-B) to quantify long-range transport of East Asian sulfur to Canada. Atmos. Chem. Phys. 8 (11), 2999–3014. http://dx.doi.org/10.5194/acp-8-2999-2008.

Weimer, S., Alfarra, M.R., Schreiber, D., Mohr, M., Prévôt, A.S.H., Baltensperger, U., 2008. Organic aerosol mass spectral signatures from wood-burning emissions: influence of burning conditions and wood type. J. Geophys. Res. 113 (D10), 1–10. http://dx.doi.org/10.1029/2007JD009309.

Zhang, Q., Jimenez, J.L., Canagaratna, M.R., Allan, J.D., Coe, H., Ulbrich, I.M., , et al.Worsnop, D.R., 2007. Ubiquity and dominance of oxygenated species in organic aerosols in anthropogenically-influenced northern hemisphere midlatitudes. Geophys. Res. Lett. 34 (13), 1–6. http://dx.doi.org/10.1029/2007GL029979.

Zhang, Q., Jimenez, J.L., Canagaratna, M.R., Ulbrich, I.M., Ng, N.L., Worsnop, D.R., Sun, Y., 2011. Understanding atmospheric organic aerosols via factor analysis of aerosol mass spectrometry: a review. Anal. Bioanal. Chem. 401 (10), 3045–3067. http://dx.doi.org/10.1007/s00216-011-5355-y.